Available online at www.sciencedirect.com

ScienceDirect

journal homepage: www.elsevier.com/locate/he

Improved room-temperature hydrogen storage performance of lithium-doped MIL-100(Fe)/graphene oxide (GO) composite

Chengbao Liu [a,b,c,1], *Dongchen Shen* [a,c,1], *Zhengkai Tu* [a,b], *Song Li* [a,b,c,*]

[a] *School of Energy and Power Engineering, Huazhong University of Science and Technology, Wuhan, 430074, China*
[b] *China-EU Institute for Clean and Renewable Energy, Huazhong University of Science and Technology, Wuhan, 430074, China*
[c] *Shenzhen Research Institute of Huazhong University of Science and Technology, Shenzhen, 518057, China*

HIGHLIGHTS

- Li^+ doped MIL-100(Fe)/GO exhibits higher hydrogen uptake than Li^+ doped MIL-100(Fe).
- The enhanced hydrogen uptake is ascribed to the high isosteric heat of adsorption.
- More ultramicropores and accessible adsorption sites exist in Li^+ doped composites.
- Li^+ ions distributed in the interface contributes most to the increased H_2 uptake.

GRAPHICAL ABSTRACT

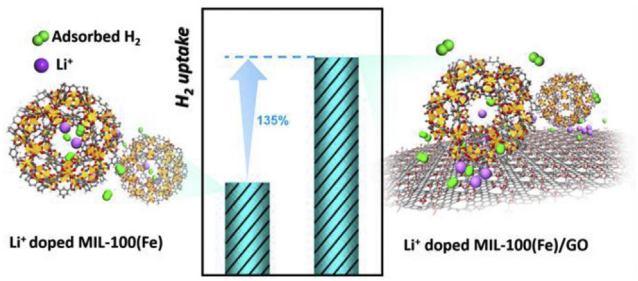

ARTICLE INFO

Article history:
Received 7 October 2021
Received in revised form
16 November 2021
Accepted 21 November 2021
Available online xxx

Keywords:
Adsorption
Metal-organic frameworks
Molecular simulation
Interaction strength
Interface

ABSTRACT

Li^+ doping is regarded as an effective strategy to enhance the room-temperature hydrogen storage of metal-organic frameworks (MOFs). In this work, Li^+ is doped into both MIL-100(Fe) and MIL-100(Fe)/graphene oxide (GO) composite, and it is demonstrated that the hydrogen uptake of Li^+ doped MIL-100(Fe)/GO (2.02 wt%) is improved by 135% compared with Li^+ doped MIL-100(Fe) (0.86 wt%) at 298 K and 50 bar, which is ascribed to its higher isosteric heat of adsorption (7.33 kJ/mol) resulting from its more accessible adsorption sites provided by doped Li^+ ions and ultramicropores. Grand canonical Monte Carlo (GCMC) simulation reveals that Li^+ ions distributing in the interface between MIL-100(Fe) and GO within MIL-100(Fe)/GO composite is favorable for hydrogen adsorption owing to the increased number of adsorption sites, thus contributing to the enhanced hydrogen storage capacity. These findings demonstrate that MIL-100(Fe)/GO is a more promising Li^+ doping substrate than MIL-100(Fe).

* *Corresponding author*. School of Energy and Power Engineering, Huazhong University of Science and Technology, Wuhan, 430074, China.
E-mail address: songli@hust.edu.cn (S. Li).
[1] These authors contributed equally to this work.
https://doi.org/10.1016/j.ijhydene.2021.11.168
0360-3199/

Introduction

Hydrogen is one of the most promising energy sources due to its high energy density, cleanliness and renewability, especially when hydrogen is produced by water electrolysis using electricity from renewable energy (e.g. solar or wind energy) [1]. From the perspective of hydrogen economy, a safe, reliable and efficient hydrogen storage strategy is of great importance for the widespread application of hydrogen energy [2,3]. Physisorption of hydrogen molecules on porous adsorbents has attracted growing research interest owing to its fast adsorption/desorption kinetics and facile reversibility [4]. Various porous adsorbents have been investigated for gas adsorption and showed great potential in hydrogen storage, including porous carbon [5–9], zeolites molecular sieve [10], metal-organic frameworks [11] and so on. But the high hydrogen storage capacity based on physisorption on porous materials is usually obtained only under cryogenic conditions (such as 77 K), which requires the utilization of expensive refrigeration systems and additional well-insulated volume to maintain an ultralow temperature [12]. Therefore, the development of high-performing materials for room temperature hydrogen storage is of great interest owing to its low cost and easy operation.

It was reported that the activated carbon could achieve high room-temperature storage capacity of 0.95 wt% at 80 bar, which was ascribed to its increased porosity and specific surface area after supercritical CO_2 activation [13]. In contrast, the hydrogen storage capacity of zeolite was usually unsatisfactory because of its high gravimetric density and relatively low specific surface area. For example, the hydrogen adsorption capacity of USY-type zeolite is only 0.4 wt% at near room temperature (30 °C) and 50 bar [14]. It has also been reported that high surface area and pore volume are favorable for physisorption performance of hydrogen molecules on porous materials [15]. Metal-organic frameworks (MOFs) are recognized as the most potential physical adsorbents for hydrogen storage due to its ultrahigh specific surface area and pore volume [16]. However, the hydrogen storage capacity of MOFs at room temperature is usually too low to meet industrial requirement. For example, the hydrogen storage capacity of MIL-101(Cr) is 0.56 wt% at 298 K and 100 bar [17], which is remarkably lower than that (7.5 wt%) at 77 K [17]. The very recently reported vanadium (II)-based MOF $V_2Cl_{2.8}$ (btdd) exhibited the hydrogen storage capacity of 1.64 wt% at 298 K and 100 bar, which exceeded the compressed storage under the same condition [18]. However, further enhancement in room-temperature hydrogen storage capacity was still in need for practical application. Although the ultrahigh surface area of MOFs is beneficial for hydrogen storage, the weak interaction between MOFs and hydrogen molecules is not favorable for room-temperature hydrogen storage [19]. Thus, enhancing the MOF-hydrogen interaction strength is the key to improve their hydrogen storage capacity at room temperature [20].

Li^+ doping has been proved effective in improving the MOF-hydrogen interaction strength, leading to the increased hydrogen storage capacity. The predicted hydrogen storage capacity of Li^+ doped MIL-101(Cr) is 10 wt% compared to 9.1 wt % of pristine MIL-101(Cr) by grand canonical Monte Carlo simulations (GCMC) at 77 K and 100 bar [21], which is attributed to the increase in isosteric heat of hydrogen adsorption from 6.6 kJ/mol to 12.0 kJ/mol. Experimental evidences have also been reported in previous studies. Li^+ doped MOF-5 exhibited an increased hydrogen storage capacity of 3.09 wt % compared to 2.49 wt% of undoped MOF-5 at 77 K and 25 atm [22], and it was speculated that Li^+ enhanced the polarizability of organic ligand, thus strengthening the charge-quadrupole interactions with hydrogen molecules. Similarly, the strong interaction between Li^+ and hydrogen molecules improved the hydrogen storage capacity of MIL-53(Al) from 0.36 wt% to 0.44 wt% at 298 K and 100 bar [17].

Moreover, it is found that Li^+ doping also favors the hydrogen storage capacity of MOF-based composites. Prabhakaran et al. [23] reported that Li^+ doped MIL-101(Cr)/single walled carbon nanotubes (SWNT) composite showed an increased hydrogen capacity of 10.43 mg/g compared to MIL-101(Cr)/SWNT (~5.5 mg/g) and Li^+ doped MIL-101(Cr) (~5.6 mg/g) at 298 K and 90 bar, which was ascribed to the strong interaction of doped Li^+ towards hydrogen molecules. Similarly, the hydrogen storage capacity of Li^+ doped MIL-101(Cr)/activated carbon (AC) composite is obviously higher (11.4 mg/g) than that of MIL-101(Cr)/AC (6.9 mg/g) at 298 K and 100 bar [24].

Graphene oxide (GO), a derivative of graphite with abundant oxygen-containing functionalities and excellent stability [25,26], is a promising functional material to integrate with MOFs for hydrogen storage. It has been reported that the high dispersion force and the additional pores generated upon GO incorporation could enhance the hydrogen adsorption capacity of MOFs [27]. The hydrogen storage capacity of Cu-BTC/GO composite (9 wt% GO) is increased to 3.58 wt% from 2.81 wt % of Cu-BTC at 77 K and 42 atm, which was contributed by the increased surface area and pore volume of the composite owing to the well-dispersion of MOF crystals [26]. Our previous work [28] demonstrated that the hydrogen storage capacity of Cu-BTC/GO was improved to 2.15 wt% from 1.51 wt% of pristine Cu-BTC at 77 K and 100 bar due to the increased pore volume of Cu-BTC/GO composites. Nevertheless, whether Li^+ doped MOF/GO composite outperforms Li^+ doped MOFs for hydrogen storage at room temperature is still elusive.

MIL-100(Fe) is one of most water-stable MOFs that can be prepared at room temperature instead of energy-intensive hydrothermal approach, enabling its low-cost and large-scale preparation for practical application [29]. However, the hydrogen storage capacity of MIL-100(Fe) is only 0.3 wt% at 298 K and 100 bar [30]. Therefore, in this work, Li^+ doped MIL-100(Fe) and MIL-100(Fe)/GO composites were successfully synthesized, and their room-temperature hydrogen storage performance was investigated by both experiments and GCMC simulations.

Methodology

Experimental

Materials

Graphite powder (325 mesh), lithium chloride (LiCl, 98%) and benzene-1,3,5-tricarboxylic acid (H_3BTC, 98%) were purchased

Please cite this article as: Liu C et al., Improved room-temperature hydrogen storage performance of lithium-doped MIL-100(Fe)/graphene oxide (GO) composite, International Journal of Hydrogen Energy, https://doi.org/10.1016/j.ijhydene.2021.11.168

from Shanghai Aladdin Bio-Chem Technology Co. Ferrous chloride tetrahydrate ($FeCl_2 \cdot 4H_2O$, 98%) was purchased from Shanghai Macklin Bio-Chem Technology Co. Potassium permanganate ($KMnO_4$, AR), hydrogen peroxide (H_2O_2, 30%), sodium nitrate ($NaNO_3$, AR), sodium hydroxide (NaOH, AR), anhydrous ethanol (AR), concentrated hydrochloric acid (HCl, AR, 37%) and concentrated sulfuric acid (H_2SO_4, AR, 98%) were purchased from Shanghai Sinopharm Chemical Reagent Co. All chemicals were used as received without any purification.

Sample preparation

MIL-100(Fe) preparation MIL-100(Fe) was synthesized under room temperature according to the literature [29]. Briefly, 3.352 g (15.2 mmol) of H_3BTC was dissolved in 45.6 ml of 1 M NaOH to form Na_3BTC solution, then 4.52 g (22.8 mmol) of $FeCl_2 \cdot 4H_2O$ was dissolved in 194.4 g deionized water to form homogeneous Fe^{2+} solution. After the solutions became completely clear of both cases, Na_3BTC solution was added dropwise over Fe^{2+} solution under stirring. The stirring was continued at room temperature for 24 h. Then the solid was recovered by centrifugation at 6000 rpm, followed by washing three times with water and ethanol, respectively. Finally, the orange solid was dried at 80 °C in air to obtain MIL-100(Fe).

GO preparation GO was prepared by a modified Hummers' method [31]. Firstly, 23 ml of concentrated sulfuric acid was placed in an ice bath for about 1 h. Then, 1 g of graphite powder and 0.5 g of $NaNO_3$ were slowly added to the concentrated sulfuric acid, and then the mixture was kept cooling for another 1 h followed by addition of 3 g of $KMnO_4$. After 30-min reaction, the ice bath was removed, 46 ml of deionized water was slowly added. Next, the solution was diluted by 140 ml deionized water and treated with 15 ml of 30% hydrogen peroxide solution and 40 ml of 10% hydrochloric acid to remove excessive MnO_4^- and MnO_2. Then, the mixture was washed with deionized water to remove residual acid and by-products until the pH of upper supernatant was neutral. Finally, the nearly pH-neutral graphite oxide was dispersed in 320 ml of deionized water under ultrasound for 40 min, then centrifuged at 2500 rpm for 30 min, the upper brown-yellow liquid was the GO suspension. Then the suspension was dried in air at 60 °C overnight to prepare solid GO sheets for further characterization.

MIL-100(Fe)/GO composite preparation MIL-100(Fe)/GO composite was synthesized *in situ* with identical precursors of MIL-100(Fe). A certain amount of GO suspension was added to Fe^{2+} solution and sonicated for 15 min to ensure fully dispersion of GO. Then Na_3BTC solution was added dropwise over Fe^{2+} solution under stirring, similar to the synthesis of MIL-100(Fe). Afterwards, the stirring was kept for 24 h at room temperature followed by washing three times with water and ethanol, respectively. Finally, the solid product was dried at 80 °C in air to remove the excessive ethanol. The amount of GO added was 1%, 2%, 5% and 10% of the mass of $FeCl_2 \cdot 4H_2O$, and the corresponding composites were named as MIL-100(Fe)/1 wt% GO, MIL-100(Fe)/2 wt% GO, MIL-100(Fe)/5 wt% GO and MIL-100(Fe)/10 wt% GO.

Li^+ doped MIL-100(Fe) and MIL-100(Fe)/GO preparation Li^+ doped MIL-100(Fe) and MIL-100(Fe)/GO were prepared by impregnation. Typically, 1 g of pre-activated MIL-100(Fe) or MIL-100(Fe)/5 wt% GO was dispersed in 100 ml anhydrous ethanol at first. Then different amounts (i.e., 0.5 ml, 1 ml and 5 ml) of 1 M LiCl/ethanol solution were added as lithium source and the solution was kept stirring under room temperature for 8 h. Finally, the solid was recovered by centrifugation at 6000 rpm and dried at 80 °C for 8 h. The obtained products with the low, medium and high content of Li^+ ions were denoted as MIL-100(Fe)/GO-L, MIL-100(Fe)/GO-M and MIL-100(Fe)/GO-H for MIL-100(Fe)/GO, and MIL-100(Fe)-L, MIL-100(Fe)-M and MIL-100(Fe)—H for MIL-100(Fe).

Characterizations

Powder X-ray diffraction (PXRD) patterns were collected on a PANalytical B.V. Empyrean diffractometer using Cu Kα (λ = 1.540598 Å) radiation at 40 kV and 40 mA. 2θ ranges from 3° to 15° as a continuous scan with a step size of 0.01313° at room temperature. **Scanning electron microscope (SEM)** was adopted to observe the crystal morphologies of materials by a field emission Nova Nano SEM 450 scanning electron microscope at an accelerating voltage of 15 kV (5 kV for GO). All samples were treated with gold coating before SEM tests. **Nitrogen adsorption isotherms** were measured at 77 K on an Autosorb-iQ2 from Quantachrome Instruments. All samples were activated at 423 K for 12 h under vacuum before measurement. Brunauer-Emmett-Teller (BET) surface areas were determined by fitting the BET model to the collected isotherms in the pressure range of $P/P_0 = 0.05—0.30$. Pore size distributions (PSD) were analyzed by quench density functional theory (QSDFT). **Fourier transform infrared spectra (FT-IR)** were obtained on a Nicolet iS50R spectrometer from Thermo Scientific Instruments with KBr pellets in the 4000—400 cm^{-1} region, approximately 1 mg of sample was mixed and ground with the appropriate amount of KBr powder before each test. **Inductively coupled plasma optical emission spectrometer (ICP-OES)** was performed on the doped materials to detected the precise content of Li^+ in the composites from Agilent ICPOES 730 instrument. Prior to ICP analysis, the samples were digested with dilute nitric acid and dilute hydrofluoric acid at 180 °C to obtain completely clear solution.

Hydrogen adsorption measurement

Hydrogen adsorption isotherms were recorded on a BELSORP-HP adsorption apparatus at 298 K and 0—50 bar. The samples for tests was about 100 mg. Before the tests, the sample was activated at 423 K for 12 h under vacuum, and the internal system was purged with helium gas followed by evacuation with vacuum pumps. The dead volume of the sample tube was therefore experimentally determined based on helium measurements to obtain corrected adsorption data. The isosteric heat of hydrogen adsorption was calculated by Clausius—Clapeyron equation (Eq. (1)) for two different isotherms measured at 298 K and 308 K.

$$Q_{st} = -RIn\left(\frac{P_1}{P_2}\right)\frac{T_1T_2}{T_2 - T_1} \quad (1)$$

where P is the equilibrium hydrogen pressure at a certain temperature T. R is the universal gas constant.

Please cite this article as: Liu C et al., Improved room-temperature hydrogen storage performance of lithium-doped MIL-100(Fe)/graphene oxide (GO) composite, International Journal of Hydrogen Energy, https://doi.org/10.1016/j.ijhydene.2021.11.168

Molecular simulations

Li^+ doped MIL-100(Fe)/GO composite model

The models of MIL-100(Fe) and GO were constructed, respectively, according to our previous study [28]. Based on the crystal surface and geometry optimization, the structure of MIL-100(Fe) [32] was altered to a surface model with the dimension of 51.552 Å × 51.552 Å × 51.552 Å, respectively. In the meantime, the one-layer GO with three -C-O-C, four −OH and two −COOH was placed parallel and expanded to fit the surface model of MIL-100(Fe). After geometry optimization using Forcite module of Materials Studio, the structure of MIL-100(Fe)/GO was obtained ultimately.

Molecular dynamics (MD) was adopted to simulate the Li^+ doping process in experiment. MIL-100(Fe)/GO was randomly inserted with ethanol molecules and a fixed number of LiCl ion pairs, which is in consistent with the experimental protocol. The ethanol molecules were gradually removed to simulate the solvent evaporation process (Fig. 1(a)–(c)) in experiment, each of which was followed by a 24-ns MD simulation. The Li^+ doped MIL-100(Fe)/GO model was finally obtained after the removal of all ethanol molecules as shown in Fig. 1(c).

MD simulations were performed using Gromacs [33]. The temperature was fixed at 298 K using a velocity scaling thermostat [34] and the relaxation time for the thermostat was 0.2 ps The Lennard-Jones (L-J) interaction and Coulombic interaction were truncated at 1.28 nm, while the PME method [35] was chosen for the long-range electrostatic interactions. 24 ns was set as the typical simulation length and the time step was 1 fs. Besides, constraints were used to freeze the atom coordinates of MIL-100(Fe) and GO.

GCMC simulations

Grand Canonical Monte Carlo (GCMC) simulations were carried out in RASPA [36] for the pristine and Li^+ doped MIL-100(Fe) as well as MIL-100(Fe)/GO to predict the hydrogen adsorption capacity. Combined with Lorentz-Berthelot mixing rules, L-J parameters taken from the universal force field (UFF) [37] were adopted for all atoms of MIL-100(Fe)/GO and MIL-100(Fe), while all the parameters of Cl^- and Li^+ were from literature [21]. All the atomic charges were obtained from the EQeq method [38]. The hydrogen molecules were described as Darkrim-Levesque (DL) model [39]. In GCMC simulation, 12.8 Å was the cutoff for L-J interactions, and the Ewald summation technique was chosen for the long-range electrostatic interactions. 6×10^4 GCMC cycles were performed including 3×10^4 cycles for equilibration and 3×10^4 cycles for production. Five types of Monte Carlo moves including translation, rotation, reinsertion, insertion and deletion were performed with equal probability. Finally, the hydrogen adsorption isotherms were obtained at 298 K and 0–50 bar.

Results and discussion

Structure analysis

The PXRD patterns of Li^+ doped MIL-100(Fe) and MIL-100(Fe)/GO in Fig. 2 are identical to that of simulated MIL-100(Fe) [40], suggesting that Li^+ doping does not disrupt the crystal structure of MIL-100(Fe). Similarly, crystallographic structure of MIL-100(Fe) was well preserved upon incorporation of GO regardless of the GO concentration (Fig. S1). The successful incorporation of GO was confirmed by the appearance of 1047 cm^{-1} peak in FT-IR of MIL-100(Fe)/GO composites (Fig. S2), corresponding to the unique C–O–C stretching vibration of GO. According to the PXRD patterns of GO and Li^+ doped MIL-100(Fe)/GO composites in Fig. 2(b), the single peak at $2\theta = 9.665^\circ$ of GO is consistent with previous report [41]. However, the characteristic peak of GO was absent in PXRD of the MIL-100(Fe)/GO composites, which may be ascribed to the high dispersion or the low amount of GO in the composites [42,43]. In addition, it was found that the peak intensity of Li^+ doped MIL-100(Fe) and MIL-100(Fe)/GO slightly decreased compared to undoped counterparts, which was possibly attributed to the reduced crystallinity of MIL-100(Fe) upon Li^+ doping. Furthermore, the diffraction peaks of doped samples were slightly shifted to the right, indicating the decreased interplanar spacing as determined by Bragg's law.

SEM images in Fig. 3 demonstrates that MIL-100(Fe) crystals exhibit an octahedral structure and smooth surface with the size of 200–300 nm, which are randomly anchored and dispersed on the winkled GO surface of MIL-100(Fe)/GO in Fig. 3(e). Besides, the complete structures of doped samples confirm that Li^+ doping does not disrupt the crystal morphology of MIL-100(Fe) (Fig. 3(d)) and MIL-100(Fe)/GO-M (Fig. 3(f)).

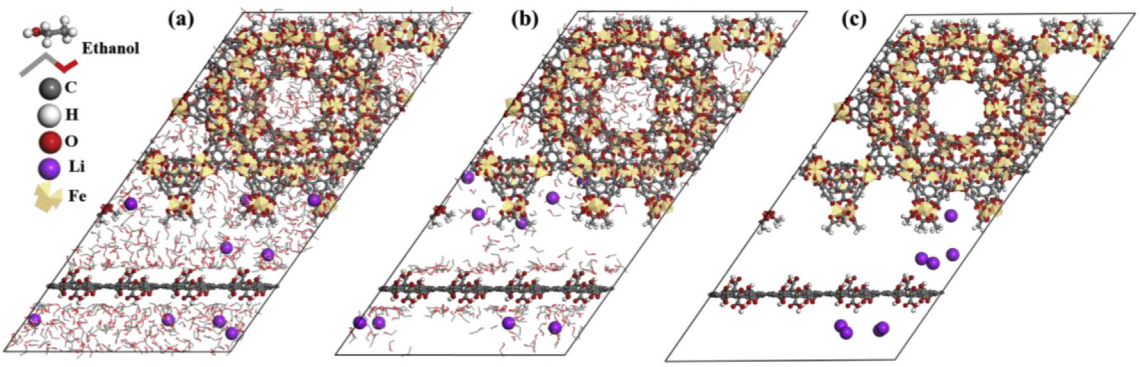

Fig. 1 – Snapshots of Li^+ doped MIL-100(Fe)/GO with abundant ethanol (a), the ethanol removing process (b) and the final Li^+ doped MIL-100(Fe)/GO without ethanol (c).

Please cite this article as: Liu C et al., Improved room-temperature hydrogen storage performance of lithium-doped MIL-100(Fe)/graphene oxide (GO) composite, International Journal of Hydrogen Energy, https://doi.org/10.1016/j.ijhydene.2021.11.168

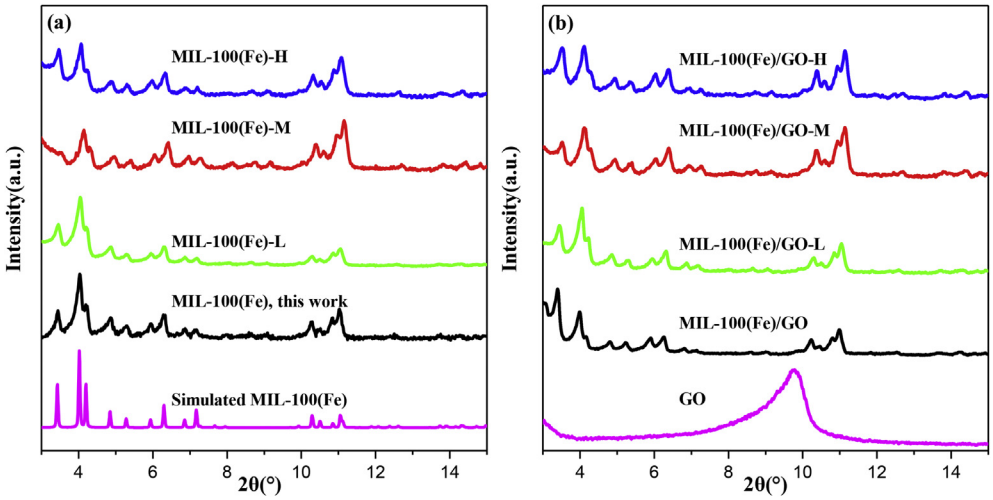

Fig. 2 – PXRD patterns of Li^+ doped MIL-100(Fe) (a) and MIL-100(Fe)/GO (b).

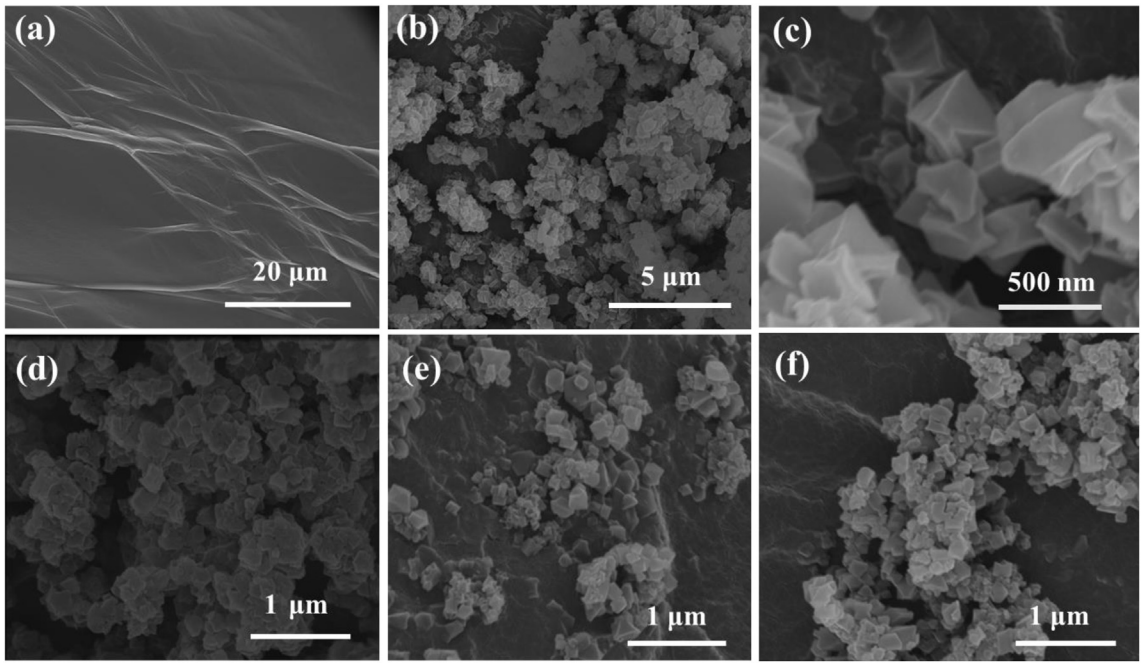

Fig. 3 – SEM images of GO (a), MIL-100(Fe) (b and c), MIL-100(Fe)-M (d), MIL-100(Fe)/GO (e) and MIL-100(Fe)/GO-M (f).

Table 1 – Textural properties of different samples.

Sample	S_{BET} (m^2/g)	V_{total} (cm^3/g)[a]	V_{micro} (cm^3/g)[b]	Li^+ content (ppm)[c]
MIL-100(Fe)	2001	1.11	0.63	–
MIL-100(Fe)-L	1869	1.06	0.59	665.5
MIL-100(Fe)-M	1784	1.01	0.56	988.8
MIL-100(Fe)–H	1654	0.94	0.51	2815.1
MIL-100(Fe)/GO	1969	1.23	0.62	–
MIL-100(Fe)/GO-L	1785	1.17	0.57	718.0
MIL-100(Fe)/GO-M	1801	1.18	0.59	1123.8
MIL-100(Fe)/GO-H	1536	1.02	0.50	2098.8

[a] Measured at P/P0 = 0.995.
[b] Calculated by t-plot.
[c] Detected by ICP-OES.

Please cite this article as: Liu C et al., Improved room-temperature hydrogen storage performance of lithium-doped MIL-100(Fe)/graphene oxide (GO) composite, International Journal of Hydrogen Energy, https://doi.org/10.1016/j.ijhydene.2021.11.168

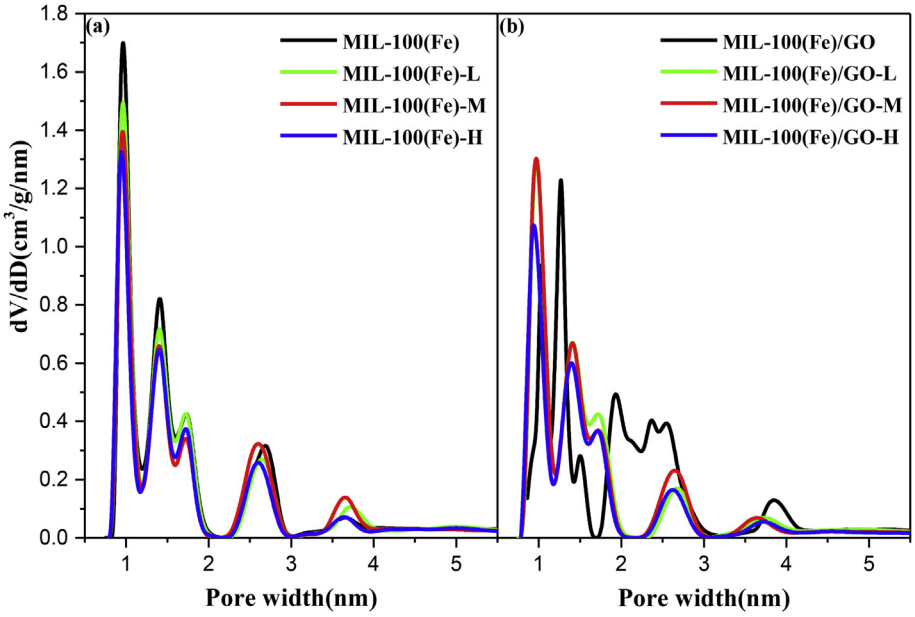

Fig. 4 – Pore size distributions of Li^+ doped MIL-100(Fe) (a) and MIL-100(Fe)/GO (b).

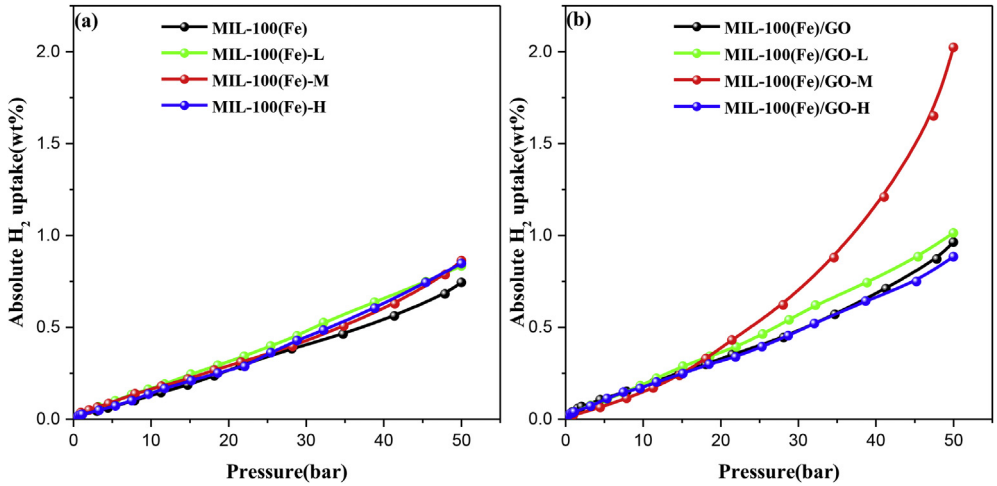

Fig. 5 – H_2 adsorption isotherms of Li^+ doped MIL-100(Fe)(a) and MIL-100(Fe)/GO(b) at 298 K.

The textural properties of samples determined by N_2 adsorption isotherms at 77 K were shown in Table 1. BET surface area of synthesized MIL-100(Fe) is 2001 m^2/g, which was slightly higher than that synthesized by conventional hydrothermal method [40,44]. Upon GO incorporation, BET surface area was decreased (1969 m^2/g) depending on GO contents (Table S1). MIL-100(Fe)/5 wt% GO shows the highest specific surface area of 1969 m^2/g, which was thus chosen for the following Li^+ doping. The low-content GO may be favorable for the nucleation of MIL-100(Fe), thus promoting the growth of crystals and increasing the surface area. In contrast, high-content GO may account for serious layer stacking, leading to the reduced surface area. Regarding the pore volume, the pore volume of MIL-100(Fe) (1.11 cm^3/g) is reduced upon Li^+ doping, which decreases with the increased Li^+ content due to the occupied space by Li^+. On the contrary, GO integration increases the pore volume of

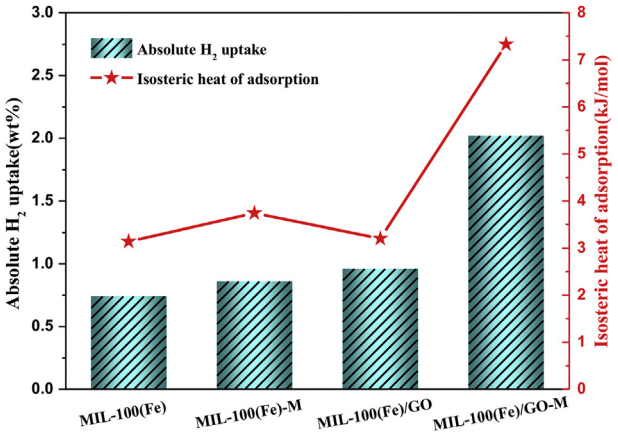

Fig. 6 – Hydrogen storage capacity and isosteric heat of hydrogen adsorption of Li^+ doped MIL-100(Fe) and MIL-100(Fe)/GO at 298 K and 50 bar.

Please cite this article as: Liu C et al., Improved room-temperature hydrogen storage performance of lithium-doped MIL-100(Fe)/graphene oxide (GO) composite, International Journal of Hydrogen Energy, https://doi.org/10.1016/j.ijhydene.2021.11.168

MIL-100(Fe) up to 1.23 cm^3/g, which is mostly resulted from the additionally generated mesopores in the interface between GO and MIL-100(Fe). The pore size distribution (PSD) in Fig. S3 also substantiated this anticipation. The reduced peak intensity of PSD in micropore region of MIL-100(Fe) (Fig. 4(a)) implicates that Li^+ mainly enters the micropores of MIL-100(Fe). Dissimilarly, both the reduced mesopore size and the peak shift towards micropore size (Fig. 4(b)) indicates that Li^+ enters not only micropores but also mesopores of MIL-100(Fe)/GO, which may favor hydrogen adsorption.

Hydrogen adsorption performance

In spite of the reduced surface area and pore volume upon Li^+ doping, the hydrogen storage performance of Li^+ doped MIL-100(Fe) and MIL-100(Fe)/GO is enhanced, especially for Li^+ doped MIL-100(Fe)/GO compared with their undoped counterparts (Fig. 5). It should be noted that the enhancement in hydrogen uptake of Li^+ doped MIL-100(Fe)/GO (Fig. 5(b)) is significantly higher than Li^+ doped MIL-100(Fe) (Fig. 5(a)), suggesting that MIL-100(Fe)/GO outperforms MIL-100(Fe) for Li^+ doping in terms of the hydrogen adsorption capacity. Although previous studies have attributed the enhancement to the strong interaction between doped Li^+ and hydrogen molecules in MOFs resulting from the charge-induced dipole interactions [22], different tendencies were observed for Li^+ doped MIL-100(Fe) and MIL-100(Fe)/GO. Such an enhancement is not remarkable for Li^+ doped MIL-100(Fe) regardless of the Li^+ content, whereas the remarkable enhancement is observed in Li^+ doped MIL-100(Fe)/GO.

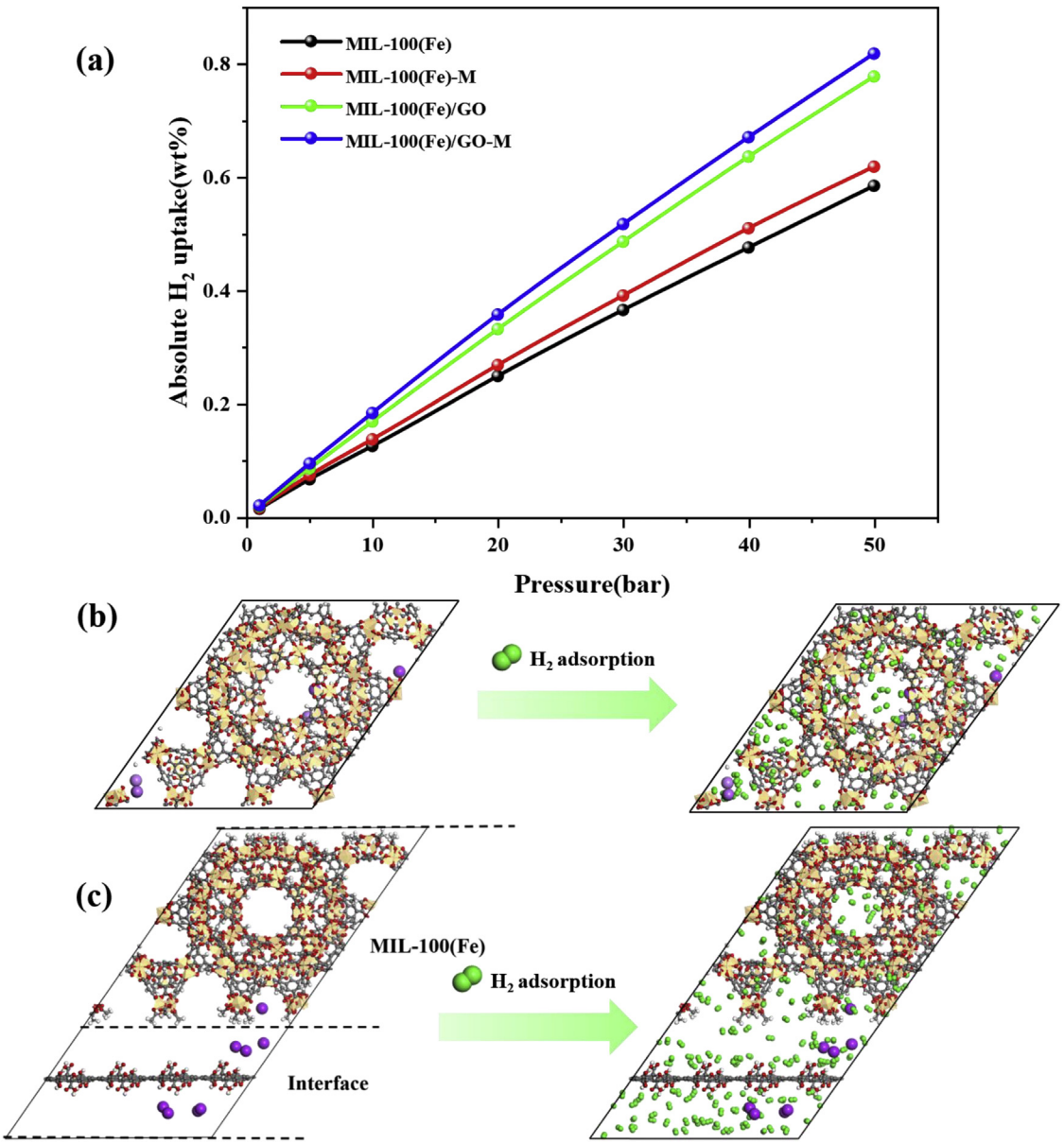

Fig. 7 – The simulated hydrogen isotherms of MIL-100(Fe), MIL-100(Fe)-M, MIL-100(Fe)/GO and MIL-100(Fe)/GO-M composite at 298 K (a); the snapshots of Li^+ doped MIL-100(Fe) (b) and MIL-100(Fe)/GO (c) before and after H_2 adsorption.

Please cite this article as: Liu C et al., Improved room-temperature hydrogen storage performance of lithium-doped MIL-100(Fe)/graphene oxide (GO) composite, International Journal of Hydrogen Energy, https://doi.org/10.1016/j.ijhydene.2021.11.168

According to the PSD of Li^+ doped MIL-100(Fe) in Fig. 4(a), the reduced peak intensity suggests the decreased pore volume and the unchanged peak position indicates the unchanged pore size upon Li^+ doping, which is mostly contributed by the aggregation of Li^+ ions in a number of micro- and mesopores of MOFs. Therefore, the insignificant enhancement in Li^+ doped MIL-100(Fe) may be ascribed to the reduced number of accessible adsorption sites for hydrogen molecules owing to the aggregation of Li^+ ions. In contrast, the shifted peaks towards smaller pore size in PSD of MIL-100(Fe)/GO composites suggested that relative uniform distribution Li^+ ions in both micropore and mesopores of composites, which may be ascribed to the presence of GO that facilitates the well distribution of Li^+ ions to provided more accessible hydrogen adsorption sites. Therefore, the interaction between Li^+ doped MIL-100(Fe)/GO and hydrogen molecules are strengthened.

Moreover, among the three composites, MIL-100(Fe)/GO-M with medium Li^+ content exhibits the highest hydrogen adsorption capacity of 2.02 wt%, followed by the MIL-100(Fe)/GO-L and MIL-100(Fe)/GO-H. The low content of Li^+ may provide insufficient adsorption sites for hydrogen molecules in MIL-100(Fe)/GO-L, whereas the high content of Li^+ may cause ion agglomeration in MIL-100(Fe)/GO-H. Both cases are not beneficial for hydrogen adsorption. Besides, the ultramicropore less than 1 nm as evidenced by PSD of Li^+ doped MIL-100(Fe)/GO of Fig. 4(b) is favorable for hydrogen uptakes [45,46] due to the overlapped potential energy of micropore walls that is able to trap hydrogen molecules [47]. Recent study revealed that the narrow interlayer distance about 0.7 nm of Ti_2CT_x MXene nanosheets could create "nanopump effect", which could efficiently improve their room-temperature hydrogen adsorption capacity [48]. Similarly, the porous activated carbon with the pore size of 0.7 nm also showed the hydrogen capacity of 1.06 wt% at 298 K and 15 bar [49], which was higher than 0.15 wt% of activated carbon with the pore size of 1–4 nm under the same condition [50]. According to PSD of Fig. 4(b), there are obviously more ultramicropores in MIL-100(Fe)/GO-M than MIL-100(Fe)/GO-L and MIL-100(Fe)/GO-H. Thus, more accessible adsorption sites provided by Li^+ ions plus a larger number of ultramicropores in MIL-100(Fe)/GO-M may favor its hydrogen adsorption through "nanopump effect" in our scenario, which will be demonstrated through their isosteric heat of adsorption later.

Comparing the hydrogen adsorption capacity of MIL-100(Fe)-M and MIL-100(Fe)/GO-M at 50 bar (Fig. 6), MIL-100(Fe)/GO-M (2.02 wt%) exhibited more than twice of hydrogen adsorption capacity of MIL-100(Fe)-M (0.86 wt%), consistent with their isosteric heat of hydrogen adsorption. The isosteric heat of hydrogen adsorption of MIL-100(Fe)/GO-M (7.33 kJ/mol) is significantly higher than MIL-100(Fe)/GO (3.20 kJ/mol) and MIL-100(Fe)-M(3.74 kJ/mol), implicating the enhanced interaction between MIL-100(Fe)/GO-M and hydrogen molecules resulting from its more ultramicropores and accessible hydrogen adsorption sites provided by Li^+. Nevertheless, the enhancement is different in Li^+ doped MIL-100(Fe) and MIL-100(Fe)/GO, which may stem from the different Li^+ ion distributions in MIL-100(Fe) and MIL-100(Fe)/GO. In order to provide molecular insights into the Li^+ distribution in MIL-100(Fe) and MIL-100(Fe)/GO, respectively, GCMC simulations were conducted for further analysis.

GCMC simulation

To explore the underlying mechanisms of the improved room-temperature hydrogen storage capacities of Li^+ doped MIL-100(Fe)/GO composite, the predicted hydrogen adsorption capacities by GCMC simulation were firstly analyzed (Fig. 7). It was found that the predicted hydrogen adsorption capacities at 298 K and 50 bar follows exactly identical trend to experimental measurements, i.e., MIL-100(Fe)/GO-M > MIL-100(Fe)/GO > MIL-100(Fe)-M > MIL-100(Fe). However, the experimental capacity was slightly higher than the simulated results, which may be ascribed to two reasons: (1) the defects in the synthesized MOFs are favorable for hydrogen adsorption [51], which is ignored in GCMC simulation; (2) experimentally synthesized GO possesses wrinkled surface that benefits the hydrogen adsorption [45,52], which is not taken into consideration in GCMC either. Moreover, it is found that the doped Li^+ ions mainly distribute in the small pores of MIL-100(Fe), while most Li^+ ions spread at the interface region between GO and MIL-100(Fe) of MIL-100(Fe)/GO composite, which provides more accessible sites for hydrogen adsorption. Such an observation is consistent with our assumption that the presence of GO facilitates the distribution of Li^+ ions to provide more accessible adsorption sites.

In order to thoroughly elucidate the mechanism of the improved hydrogen storage capacity in MIL-100(Fe)/GO-M, the number of adsorbed hydrogen molecules in MOF frameworks and interface regions were analyzed (Fig. 8). It is found that 41.31% of hydrogen molecules are in the interface region of MIL-100(Fe)/GO-M, leading to the remarkably increased hydrogen adsorption capacity compared with MIL-100(Fe)-M. Although both Li^+ doping and GO incorporation are favorable for hydrogen adsorption, Li^+ doping plays a dominant role for MIL-100(Fe)/GO-M in experiment (Fig. 6). However, GO incorporation contributes most to the hydrogen uptake of MIL-100(Fe)/GO-M compared with the undoped MIL-100(Fe)/GO, which may be ascribed to the ideal GO model in the MIL-100(Fe)/GO composite of GCMC simulations.

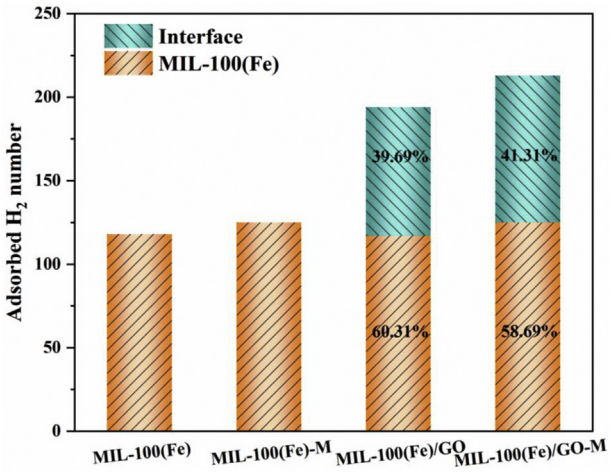

Fig. 8 – The number of adsorbed H_2 in framework and MOF-GO interface of MIL-100(Fe), MIL-100(Fe)-M, MIL-100(Fe)/GO and MIL-100(Fe)/GO-M composite.

Please cite this article as: Liu C et al., Improved room-temperature hydrogen storage performance of lithium-doped MIL-100(Fe)/graphene oxide (GO) composite, International Journal of Hydrogen Energy, https://doi.org/10.1016/j.ijhydene.2021.11.168

Conclusions

In this work, the room-temperature hydrogen storage performance of Li^+ doped MIL-100(Fe) and MIL-100(Fe)/GO were investigated by combined experimental and simulation approach. It was demonstrated that although Li^+ doping can effectively improve the room-temperature hydrogen storage capacity of both MIL-100(Fe) and MIL-100(Fe)/GO, Li^+ doped MIL-100(Fe)/GO exhibited remarkably higher hydrogen adsorption capacity (2.02 wt%) than Li^+ doped MIL-100(Fe) (0.86 wt%) at 298 K and 50 bar. The enhancement was ascribed to the strengthened MOF-hydrogen interaction or the isosteric heat of adsorption contributed by the larger number of ultramicropores and more accessible adsorption sites provided by uniformly distributed Li^+ ions in pores. The underlying mechanism of the remarkable improvement in hydrogen storage capacity of Li^+ doped MIL-100(Fe)/GO was further revealed by GCMC simulations, in which a considerable amount of Li^+ ions distributed in the interface between GO and MIL-100(Fe) contributes over 40% hydrogen uptake of Li^+ doped MIL-100(Fe)/GO-M by providing additional hydrogen adsorption sites. This work reported a novel strategy to improve the room-temperature hydrogen storage of MIL-100(Fe) by Li^+ doping of MIL-100(Fe)/GO composites, which may be also extended to other MOFs. In addition, the molecular mechanism for improved hydrogen storage disclosed in this work may be applicable to other Li^+ doped MOF/GO composites. This work may also inspire further exploration of high-performing room-temperature hydrogen storage adsorbents based on MOF/GO composites.

Declaration of competing interest

The authors declare that they have no known competing financial interests or personal relationships that could have appeared to influence the work reported in this paper.

Acknowledgments

This work was funded by the Basic Research Foundation of Shenzhen (No. JCYJ20190809101403595). We thank the support from Analytical & Testing Center of Huazhong University of Science and Technology.

Appendix A. Supplementary data

Supplementary data to this article can be found online at https://doi.org/10.1016/j.ijhydene.2021.11.168.

REFERENCES

[1] Ji M, Wang J. Review and comparison of various hydrogen production methods based on costs and life cycle impact assessment indicators. Int J Hydrogen Energy 2021;46:38612–35.
[2] Shet SP, Shanmuga Priya S, Sudhakar K, Tahir M. A review on current trends in potential use of metal-organic framework for hydrogen storage. Int J Hydrogen Energy 2021;46:11782–803.
[3] Attia NF, Jung M, Park J, Cho S-Y, Oh H. Facile synthesis of hybrid porous composites and its porous carbon for enhanced H2 and CH4 storage. Int J Hydrogen Energy 2020;45:32797–807.
[4] Gangu KK, Maddila S, Mukkamala SB, Jonnalagadda SB. Characteristics of MOF, MWCNT and graphene containing materials for hydrogen storage: a review. J Energy Chem 2019;30:132–44.
[5] Park J, Cho SY, Jung M, Lee K, Nah Y-C, Attia NF, et al. Efficient synthetic approach for nanoporous adsorbents capable of pre- and post-combustion CO2 capture and selective gas separation. J CO2 Util 2021;45:101404.
[6] Kim S, Cho SY, Son K, Attia NF, Oh H. A metal-doped flexible porous carbon cloth for enhanced CO2/CH4 separation. Separ Purif Technol 2021;277:119511.
[7] Jung M, Park J, Cho SY, Elashery SEA, Attia NF, Oh H. Flexible carbon sieve based on nanoporous carbon cloth for efficient CO2/CH4 separation. Surf Interfaces 2021;23:100960.
[8] Park J, Attia NF, Jung M, Lee K, Oh H. Biobased derived nanoporous carbon for hydrogen isotope separation. Microporous Mesoporous Mater 2020;304:109291.
[9] Jung M, Park J, Lee K, Attia NF, Oh H. Effective synthesis route of renewable nanoporous carbon adsorbent for high energy gas storage and CO2/N2 selectivity. Renew Energy 2020;161:30–42.
[10] Ozturk Z. Hydrogen storage on lithium modified silica based CHAbazite type zeolite, A computational study. Int J Hydrogen Energy 2018;43:22365–76.
[11] Cao Y, Dhahad HA, Zare SG, Farouk N, Anqi AE, Issakhov A, et al. Potential application of metal-organic frameworks (MOFs) for hydrogen storage: simulation by artificial intelligent techniques. Int J Hydrogen Energy 2021;46:36336–47.
[12] Kapelewski MT, Runcevski T, Tarver JD, Jiang HZH, Hurst KE, Parilla PA, et al. Record high hydrogen storage capacity in the metal-organic framework Ni2(m-dobdc) at near-ambient temperatures. Chem Mater 2018;30:8179–89.
[13] Xia K, Hu J, Jiang J. Enhanced room-temperature hydrogen storage in super-activated carbons: the role of porosity development by activation. Appl Surf Sci 2014;315:261–7.
[14] Chung K-H. High-pressure hydrogen storage on microporous zeolites with varying pore properties. Energy 2010;35:2235–41.
[15] Frost H, Snurr RQ. Design requirements for metal-organic frameworks as hydrogen storage materials. J Phys Chem C 2007;111:18794–803.
[16] Suh MP, Park HJ, Prasad TK, Lim DW. Hydrogen storage in metal-organic frameworks. Chem Rev 2012;112:782–835.
[17] Karikkethu Prabhakaran P, Deschamps J. Hydrogen adsorption in lithium doped MIL-101 and MIL-53(Al) at 77 and 298 K up to 100 bar: effect of lithium concentration. J Porous Mater 2015;22:1073–81.
[18] Jaramillo DE, Jiang HZH, Evans HA, Chakraborty R, Furukawa H, Brown CM, et al. Ambient-temperature hydrogen storage via vanadium(II)-Dihydrogen complexation in a metal-organic framework. J Am Chem Soc 2021;143:6248–56.
[19] Li Y, Yang RT. Gas adsorption and storage in Metal–Organic framework MOF-177. Langmuir 2007;23:12937–44.
[20] Bhatia SK, Myers AL. Optimum conditions for adsorptive storage. Langmuir 2006;22:1688–700.

[21] Ghoufi A, Deschamps J, Maurin G. Theoretical hydrogen cryostorage in doped MIL-101(Cr) metal–organic frameworks. J Phys Chem C 2012;116:10504–9.
[22] Chu C-L, Chen J-R, Lee T-Y. Enhancement of hydrogen adsorption by alkali-metal cation doping of metal-organic framework-5. Int J Hydrogen Energy 2012;37:6721–6.
[23] Prabhakaran PK, Deschamps J. Room temperature hydrogen uptake in single walled carbon nanotubes incorporated MIL-101 doped with lithium: effect of lithium doping. J Porous Mater 2015;22:1635–42.
[24] Karikkethu Prabhakaran P, Deschamps J. Doping activated carbon incorporated composite MIL-101 using lithium: impact on hydrogen uptake. J Mater Chem A 2015;3:7014–21.
[25] Taheri Z, Nakhaei Pour A. Studying of the adsorption and diffusion behaviors of methane on graphene oxide by molecular dynamics simulation. J Mol Model 2021;27:59.
[26] Liu S, Sun L, Xu F, Zhang J, Jiao C, Li F, et al. Nanosized Cu-MOFs induced by graphene oxide and enhanced gas storage capacity. Energy Environ Sci 2013;6:818–23.
[27] Petit C, Bandosz TJ. Engineering the surface of a new class of adsorbents: metal-organic framework/graphite oxide composites. J Colloid Interface Sci 2015;447:139–51.
[28] Ren W, Zhuang X, Liu Z, Li S. Hydrogen adsorption performance of Cu-BTC/graphene aerogel composite: a combined experimental and computational study. Int J Hydrogen Energy 2021;46:13097–105.
[29] Guesh K, Caiuby CAD, Mayoral Á, Díaz-García M, Díaz I, Sanchez-Sanchez M. Sustainable preparation of MIL-100(Fe) and its photocatalytic behavior in the degradation of methyl orange in water. Cryst Growth Des 2017;17:1806–13.
[30] Orcajo G, Montes-Andrés H, Villajos JA, Martos C, Botas JA, Calleja G. Li-Crown ether complex inclusion in MOF materials for enhanced H2 volumetric storage capacity at room temperature. Int J Hydrogen Energy 2019;44:19285–93.
[31] William S, Hummers J, Offeman RE. Preparation of graphitic oxide. J Am Chem Soc 1958;1339.
[32] Horcajada P, Surble S, Serre C, Hong DY, Seo YK, Chang JS, et al. Synthesis and catalytic properties of MIL-100(Fe), an iron(III) carboxylate with large pores. Chem Commun 2007:2820–2.
[33] Abraham MJ, Murtola T, Schulz R, Páll S, Smith JC, Hess B, et al. GROMACS: high performance molecular simulations through multi-level parallelism from laptops to supercomputers. SoftwareX 2015;1–2:19–25.
[34] Bussi G, Donadio D, Parrinello M. Canonical sampling through velocity rescaling. J Chem Phys 2007;126:14101.
[35] Essmann U, Perera L, Berkowitz ML, Darden T, Lee H, Pedersen LG. A smooth particle mesh Ewald method. J Chem Phys 1995;103:8577–93.
[36] Dubbeldam D, Calero S, Ellis DE, Snurr RQ. RASPA: molecular simulation software for adsorption and diffusion in flexible nanoporous materials. Mol Simulat 2016;42:81–101.
[37] Rappé AK, Casewit CJ, Colwell K, Goddard III WA, Skiff WM. UFF, a full periodic table force field for molecular mechanics and molecular dynamics simulations. J Am Chem Soc 1992;114:10024–35.
[38] Wilmer CE, Kim KC, Snurr RQ. An extended charge equilibration method. J Phys Chem Lett 2012;3:2506–11.
[39] Darkrim F, Levesque D. Monte Carlo simulations of hydrogen adsorption in single-walled carbon nanotubes. J Chem Phys 1998;109:4981–4.
[40] Simon MA, Anggraeni E, Soetaredjo FE, Santoso SP, Irawaty W, Thanh TC, et al. Hydrothermal synthesize of HF-free MIL-100(Fe) for isoniazid-drug delivery. Sci Rep 2019;9:16907.
[41] Liu Y, Xia X, Tan Y, Li S. O_2/N_2 separation performance of MIL-101(Cr)/Graphene oxide. Acta Chim Sinica 2020;78:250–5.
[42] Zhou H, Zhang J, Zhang J, Yan X-F, Shen X-P, Yuan A-H. Spillover enhanced hydrogen storage in Pt-doped MOF/graphene oxide composite produced via an impregnation method. Inorg Chem Commun 2015;54:54–6.
[43] Pokhrel J, Bhoria N, Wu C, Reddy KSK, Margetis H, Anastasiou S, et al. Cu- and Zr-based metal organic frameworks and their composites with graphene oxide for capture of acid gases at ambient temperature. J Solid State Chem 2018;266:233–43.
[44] Zhang F, Shi J, Jin Y, Fu Y, Zhong Y, Zhu W. Facile synthesis of MIL-100(Fe) under HF-free conditions and its application in the acetalization of aldehydes with diols. Chem Eng J 2015;259:183–90.
[45] Yushin G, Dash R, Jagiello J, Fischer JE, Gogotsi Y. Carbide-Derived carbons: effect of pore size on hydrogen uptake and heat of adsorption. Adv Funct Mater 2006;16:2288–93.
[46] Geng Z, Zhang C, Wang D, Zhou X, Cai M. Pore size effects of nanoporous carbons with ultra-high surface area on high-pressure hydrogen storage. J Energy Chem 2015;24:1–8.
[47] Yang S, Lin X, Blake AJ, Walker GS, Hubberstey P, Champness NR, et al. Cation-induced kinetic trapping and enhanced hydrogen adsorption in a modulated anionic metal-organic framework. Nat Chem 2009;1:487–93.
[48] Liu S, Liu J, Liu X, Shang J, Xu L, Yu R, et al. Hydrogen storage in incompletely etched multilayer Ti2CTx at room temperature. Nat Nanotechnol 2021;16:331–6.
[49] Samantaray SS, Mangisetti SR, Ramaprabhu S. Investigation of room temperature hydrogen storage in biomass derived activated carbon. J Alloys Compd 2019;789:800–4.
[50] Liu X, Zhang C, Geng Z, Cai M. High-pressure hydrogen storage and optimizing fabrication of corncob-derived activated carbon. Microporous Mesoporous Mater 2014;194:60–5.
[51] Wang C-Y, Tsao C-S, Yu M-S, Liao P-Y, Chung T-Y, Wu H-C, et al. Hydrogen storage measurement, synthesis and characterization of metal–organic frameworks via bridged spillover. J Alloys Compd 2010;492:88–94.
[52] Nishihara H, Simura T, Kyotani T. Enhanced hydrogen spillover to fullerene at ambient temperature. Chem Commun 2018;54:3327–30.

Please cite this article as: Liu C et al., Improved room-temperature hydrogen storage performance of lithium-doped MIL-100(Fe)/graphene oxide (GO) composite, International Journal of Hydrogen Energy, https://doi.org/10.1016/j.ijhydene.2021.11.168